Alignment statistics of pressure Hessian with strain rate tensor and reactive scalar gradient in turbulent premixed flames

Cite as: Phys. Fluids **34**, 065120 (2022); https://doi.org/10.1063/5.0095389
Submitted: 10 April 2022 • Accepted: 21 May 2022 • Accepted Manuscript Online: 23 May 2022 • Published Online: 09 June 2022

Published open access through an agreement with JISC Collections

Nilanjan Chakraborty, Umair Ahmed, Markus Klein, et al.

Physics of Fluids ARTICLE scitation.org/journal/phf

Alignment statistics of pressure Hessian with strain rate tensor and reactive scalar gradient in turbulent premixed flames

Cite as: Phys. Fluids **34**, 065120 (2022); doi: 10.1063/5.0095389
Submitted: 10 April 2022 · Accepted: 21 May 2022 ·
Published Online: 9 June 2022

Nilanjan Chakraborty,[1,a)] Umair Ahmed,[1] Markus Klein,[2] and Hong G. Im[3]

AFFILIATIONS

[1]School of Engineering, University of Newcastle, Claremont Road, Newcastle-Upon-Tyne NE1 7RU, United Kingdom
[2]Department of Aerospace Engineering, University of the Bundeswehr Munich, 85577 Neubiberg, Germany
[3]Clean Combustion Research Center, King Abdullah University of Science and Technology, Thuwal 23955-6900, Saudi Arabia

Note: This paper is part of the special topic, Development and Validation of Models for Turbulent Reacting Flows.
[a)]**Author to whom correspondence should be addressed:** nilanjan.chakraborty@newcastle.ac.uk

ABSTRACT

The relative alignment of the eigenvectors of pressure Hessian with reactive scalar gradient and strain rate eigenvectors in turbulent premixed flames have been analyzed for Karlovitz number values ranging from 0.75 to 126 using a detailed chemistry three-dimensional direct numerical simulations database of H_2–air premixed flames. The reactive scalar gradient preferentially aligns with the most extensive strain rate eigendirection for large Damköhler number and small Karlovitz number values, whereas a preferential collinear alignment between the reactive scalar gradient with the most compressive strain rate eigendirection is observed in flames with small Damköhler number and large Karlovitz number. By contrast, the eigenvectors of pressure Hessian do not perfectly align with the reactive scalar gradient, and the net effect of the pressure Hessian on the evolution of the normal strain rate contribution to the scalar dissipation rate transport acts to reduce the scalar gradient in the zone of high dilatation rate. The eigenvectors of pressure Hessian and the strain rate are aligned in such a manner that the contribution of pressure Hessian to the evolution of principal strain rates tends to augment the most extensive principal strain rate for small and moderate values of Karlovitz numbers, whereas this contribution plays an important role for the evolution of the intermediate principal strain rate for large values of Karlovitz number. As the reactive scalar gradient does not align with the intermediate strain rate eigenvector, the influence of pressure Hessian contributions to the scalar–turbulence interaction remains weak for large values of Karlovitz number.

I. INTRODUCTION

In premixed flames, the flow acceleration across the flame due to thermal expansion gives rise to a self-induced pressure gradient within the flame front.[1–3] This pressure gradient ∇p within the flame brush is known to have significant influences on turbulent scalar flux,[2,3] turbulent kinetic energy,[3–6] and enstrophy[3,7–10] evolutions in premixed turbulent combustion. In comparison, limited attention has been given to the statistics of the pressure Hessian tensor $\mathbf{\Pi}$ (i.e., $\Pi_{ij} = \partial^2 p/\partial x_i \partial x_j$ are the components of the pressure Hessian tensor) and its alignment with local principal strain rates in turbulent premixed flames although this aspect was analyzed in detail for non-reacting turbulent flows,[11–14] especially for homogeneous isotropic turbulence[11,13] and homogeneous axisymmetric turbulence.[14]

To appreciate the importance of pressure Hessian, consider the transport equation of the strain rate tensor with components $S_{ij} = 0.5\left(\partial u_i/\partial x_j + \partial u_j/\partial x_i\right)$, where u_i is the ith component of fluid velocity,

$$\frac{\partial S_{ij}}{\partial t} + u_k \frac{\partial S_{ij}}{\partial x_k} = -S_{ik}S_{kj} - \frac{\left(\omega_i\omega_j - \delta_{ij}\omega_k\omega_k\right)}{4} + \frac{1}{2\rho^2}\left(\frac{\partial p}{\partial x_i}\frac{\partial \rho}{\partial x_j} + \frac{\partial p}{\partial x_j}\frac{\partial \rho}{\partial x_i}\right) - \frac{\Pi_{ij}}{\rho} - \frac{1}{2\rho^2}\left(\frac{\partial p}{\partial x_i}\frac{\partial \tau_{jk}}{\partial x_k} + \frac{\partial p}{\partial x_j}\frac{\partial \tau_{ik}}{\partial x_k}\right) + \frac{1}{2\rho}\left(\frac{\partial^2 \tau_{ik}}{\partial x_j \partial x_k} + \frac{\partial^2 \tau_{ik}}{\partial x_i \partial x_k}\right). \quad (1)$$

Here, ρ is density, $\omega_i = \epsilon_{ijk}\partial u_k/\partial x_j$ is the ith component of vorticity, and $\tau_{ik} = 2\mu S_{ik} - 2\mu\delta_{ik}S_{ll}/3$ is the component of the viscous stress tensor with μ being the dynamic viscosity. Equation (1) shows that the pressure Hessian components Π_{ij} play a role in the evolution of strain rate components. In particular, $\hat{\boldsymbol{\Pi}} = \boldsymbol{E}^T\boldsymbol{\Pi}\boldsymbol{E}$ was found to play a key role in the evolution of principal strain rates in turbulent premixed flames,[15,16] where $\boldsymbol{E} = [\hat{e}_\alpha\, \hat{e}_\beta\, \hat{e}_\gamma]$ with $\hat{e}_\alpha$ ($\hat{e}_\gamma$) being the eigenvector associated with the most extensive (compressive) principal strain rate and $\hat{e}_\beta$ is the eigenvector corresponding to the intermediate strain rate. Moreover, the dissipation rate of kinetic energy is given by $\varepsilon = \tau_{ik}S_{ik}$, and thus, it can be understood from Eq. (1) that the inner product between the pressure Hessian tensor and the strain rate tensor (i.e., $\Pi_{ik}S_{ik}$) plays an important role in the evolution of ε.

Ahmed and Prosser[17,18] demonstrated that the relative alignment of the eigenvectors of the pressure Hessian tensor $\boldsymbol{\Pi}$ with the flame normal vector $\boldsymbol{N}$ affects the evolution of the scalar–turbulence interaction term (i.e., the normal strain rate $a_N = N_iN_jS_{ij}$ contribution to the scalar dissipation rate transport) $\overline{\rho}\tilde{\Delta}_c = \overline{2\rho D_c N_i N_j S_{ij}|\nabla c|^2} = \overline{2\rho D_c a_N|\nabla c|^2}$, where ρ is the gas density, c is the reaction progress variable, D_c is the reaction progress variable diffusivity, and the overbar (tilde) suggests a Reynolds (Favre) averaging/filtering operation, as appropriate. The transport equation of $\tilde{\Delta}_c$ takes the following form:[18]

$$\begin{aligned}\overline{\rho}\left[\frac{\partial\tilde{\Delta}_c}{\partial t} + \tilde{u}_j\frac{\partial\tilde{\Delta}_c}{\partial x_j}\right] &= -\frac{\partial}{\partial x_n}\left(\overline{\rho D_c u_n \frac{\partial c}{\partial x_i}S_{ij}\frac{\partial c}{\partial x_j}}\right)\\ &\quad + 2\overline{\frac{\partial c}{\partial x_i}S_{ij}\frac{\partial}{\partial x_j}\left(\frac{\partial}{\partial x_k}\left(\rho D_c^2\frac{\partial c}{\partial x_k}\right)\right)}\\ &\quad + \overline{D_c\frac{\partial c}{\partial x_i}\frac{\partial c}{\partial x_j}\frac{\partial}{\partial x_k}\left(\frac{\partial\tau_{ik}}{\partial x_j}\right)} + F_{11} + F_{12}\\ &\quad + F_2 + F_3 + F_4. \end{aligned} \tag{2}$$

Here, F_{11} is the reaction rate contribution, $F_{12} = \overline{-2D_c\Pi_{ij}N_iN_j|\nabla c|^2}$ is the contribution of pressure Hessian, and the terms F_2, F_3, and F_4 arise due to turbulent transport, dilatation rate, and turbulent straining, respectively. A positive value of F_{12} acts to increase (decrease) the magnitude of the positive (negative) value of $\tilde{\Delta}_c$, which is indicative of the increased (decreased) extent of collinear alignment between $\boldsymbol{N}$ and $\hat{e}_\alpha$ ($\hat{e}_\gamma$). The remaining terms F_{11}, F_2, F_3, and F_4 are not important for the current analysis and, thus, are not provided here, but interested readers are referred to Ref. 18 for further information in this regard. Gonzalvez and Paranthoën[19,20] concluded from their inviscid flow analysis that the anisotropy of vorticity and pressure Hessian is responsible for the modification of the scalar gradient alignments with strain rate eigenvectors from a preferential alignment of ∇c with $\hat{e}_\gamma$ in the case of passive scalar mixing to a preferential alignment of ∇c with $\hat{e}_\alpha$ in turbulent premixed flames when the heat release effects overwhelm turbulent straining.[21] Moreover, Keylock[22] argued that the pressure Hessian is a major contributor to the non-local effects on the vorticity and scalar gradient alignments in turbulent flows.

All the aforementioned information indicates that the statistics of the alignment of pressure Hessian with strain rate eigenvectors and reactive scalar gradient are important for the analysis of turbulent premixed flame physics, but this aspect is yet to be analyzed in detail. This paper addresses this gap in the existing literature by analyzing the pressure Hessian statistics using detailed chemistry Direct Numerical Simulation (DNS) data of statistically planar H_2–air flames with an equivalence ratio of $\phi = 0.7$ for different turbulence intensities across different combustion regimes. The main objectives of the current analysis are (i) to demonstrate the effects of turbulence intensity and regime of combustion on the alignment of pressure Hessian with local principal strain rate eigenvectors, and ∇c, and (ii) to explain the observed behavior based on physical principles and provide modeling implications.

II. MATHEMATICAL AND NUMERICAL BACKGROUND

The components of $\hat{\boldsymbol{\Pi}} = \boldsymbol{E}^T\boldsymbol{\Pi}\boldsymbol{E}$ in the strain rate eigendirections (i.e., $\hat{\Pi}_\alpha$, $\hat{\Pi}_\beta$, and $\hat{\Pi}_\gamma$) are given as[16]

$$\hat{\Pi}_\alpha = \Pi_\alpha\cos^2(\hat{\pi}_\alpha,\hat{e}_\alpha) + \Pi_\beta\cos^2(\hat{\pi}_\beta,\hat{e}_\alpha) + \Pi_\gamma\cos^2(\hat{\pi}_\gamma,\hat{e}_\alpha), \tag{3a}$$

$$\hat{\Pi}_\beta = \Pi_\alpha\cos^2(\hat{\pi}_\alpha,\hat{e}_\beta) + \Pi_\beta\cos^2(\hat{\pi}_\beta,\hat{e}_\beta) + \Pi_\gamma\cos^2(\hat{\pi}_\gamma,\hat{e}_\beta), \tag{3b}$$

$$\hat{\Pi}_\gamma = \Pi_\alpha\cos^2(\hat{\pi}_\alpha,\hat{e}_\gamma) + \Pi_\beta\cos^2(\hat{\pi}_\beta,\hat{e}_\gamma) + \Pi_\gamma\cos^2(\hat{\pi}_\gamma,\hat{e}_\gamma), \tag{3c}$$

where Π_α, Π_β, and Π_γ are the most extensive, intermediate, and the most compressive eigenvalues of the pressure Hessian and $\hat{\pi}_\alpha, \hat{\pi}_\beta$, and $\hat{\pi}_\gamma$ are the corresponding eigenvectors. Similarly, the contribution of $F_{12} = \overline{-2D_c\Pi_{ij}N_iN_j|\nabla c|^2}$ in the transport equation of $\tilde{\Delta}_c$ [see Eq. (2)] can be expressed as[18]

$$\begin{aligned}F_{12} &= \overline{-2D_c\Pi_{ij}N_iN_j|\nabla c|^2}\\ &= \overline{-2D_c|\nabla c|^2[\Pi_\alpha\cos^2(\hat{\pi}_\alpha,\mathbf{N}) + \Pi_\beta\cos^2(\hat{\pi}_\beta,\mathbf{N}) + \Pi_\gamma\cos^2(\hat{\pi}_\gamma,\mathbf{N})]}. \end{aligned} \tag{4}$$

The flame normal vector $\boldsymbol{N}$ is defined as $\boldsymbol{N} = -\nabla c/|\nabla c|$, where the reaction progress variable c is defined based on a suitable species mass fraction Y_α as $c = (Y_{\alpha 0} - Y_\alpha)/(Y_{\alpha 0} - Y_{\alpha\infty})$, where subscripts 0 and ∞ refer to the values in the unburned gas and fully burned products, respectively. For the present analysis, $\alpha = H_2, O_2$, and H_2O have been used, but the qualitative nature of the pressure Hessian statistics does not depend on the choice of the definition of c. It is also possible to define a non-dimensional temperature c_T as $c_T = (T - T_0)/(T_{ad} - T_0)$, where T_0 and T_{ad} are the unburned gas temperature and adiabatic flame temperature, respectively. In the context of multi-step chemistry, $c = c_T$ is not necessarily maintained, and this assumption does not play any role in the analysis conducted in this paper.

It can be appreciated from Eqs. (3) and (4) that the relative alignments of pressure Hessian with strain rate eigenvectors and ∇c are important for the analysis of fluid turbulence in premixed combustion. These statistics have been explored in this paper for H_2–air premixed flames with an equivalence ratio ϕ of 0.7 (i.e., $\phi = 0.7$) using a three-dimensional DNS database,[10,23] which uses a detailed chemical mechanism[24] with 9 species and 19 chemical reactions. H_2–air premixed flames with an equivalence ratio ϕ of 0.7 are thermo-diffusively neutral in terms of stretch rate effects.[25,26] Therefore, the effects of differential diffusion are relatively weak for $\phi = 0.7$ in the case of H_2–air premixed flames. For this database, the unburned gas temperature T_0 is taken to be 300 K, which yields an unstrained laminar burning velocity $S_L = 135.6$ cm/s under atmospheric pressure. Turbulent inflow and outflow boundaries are considered in the direction of mean flame propagation and are specified using the Navier–Stokes characteristic boundary conditions technique, and transverse boundaries are

taken to be periodic. High order finite-difference (eighth order for the internal grid points) and third order explicit Runge–Kutta schemes are used for numerical differentiation and explicit time advancement, respectively, and the interested readers are referred elsewhere[10,23] for detailed information on numerical implementation. The mean inlet velocity has been gradually modified as the simulation progresses to match the turbulent burning velocity, so that a statistically stationary state can be obtained. The inflow values of normalized root mean square turbulent velocity fluctuation u'/S_L, the most energetic turbulent length scale to flame thickness ratio l_T/δ_{th}, the Damköhler number $Da = l_T S_L/u'\delta_{th}$, the Karlovitz number $Ka = (\rho_0 S_L \delta_{th}/\mu_0)^{0.5}(u'/S_L)^{1.5}(l_T/\delta_{th})^{-0.5}$, and the turbulent Reynolds number $Re_t = \rho_0 u' l_T/\mu_0$ for all cases are listed in Table I, where ρ_0 is the unburned gas density, μ_0 is the unburned gas viscosity, $\delta_{th} = (T_{ad} - T_0)/\max|\nabla T|_L$ is the thermal flame thickness, and the subscript "L" is used to refer to the unstrained laminar flame quantities. The longitudinal integral scale L_{11} is a factor of 2.5 smaller than the most energetic scale l_T, and thus, the values of Ka (Da) in Table I increase (decrease) by a factor of 1.6 (2.5) if L_{11} instead of l_T is used for their definitions. For cases A and B (case C), the domain size is taken to be $20 \times 10 \times 10\,\text{mm}^3$ ($8 \times 2 \times 2\,\text{mm}^3$), which has been discretized by a uniform Cartesian grid of dimension $512 \times 256 \times 256$ ($1280 \times 320 \times 320$). The simulation time corresponds to $\{2.5,\ 17,\ 16.75\}L_{11}/u'$ for cases A–C, respectively, and is comparable to several previous analyses.[2,4,5,27,28] The cases investigated here belong to the corrugated flamelets (i.e., case A with $Ka < 1$), thin reaction zones (i.e., case B with $1 < Ka < 100$), and broken reaction zones (i.e., case C with $Ka > 100$) regimes according to Peters.[29] Whether the broken reaction zones combustion is realized in case C is not the focus of this analysis, and without doubt, cases A–C allow for the analysis of the effects of Ka on the pressure Hessian statistics. In this regard, it is worthwhile to note that most practical combustion devices operate within the corrugated and thin reaction zones combustion regimes,[30] and the upper range of Ka in conventional engines remains about 13.0.[31] However, in lean premixed prevaporized (LPP) gas turbine combustors[32] and some laboratory-scale configurations[33] using lean hydrocarbon flames, Ka values can be high especially under elevated pressure and can locally reach close to the $Ka = 100$ boundary. The $Ka > 100$ conditions are also likely in next generation combustors involving NH_3 combustion.[34]

III. RESULTS AND DISCUSSION

The distributions of vorticity, flow topology, and scalar gradient within the flame-front for cases A–C are presented elsewhere[3,10,23] and, thus, will not be repeated here. However, the distribution of the $\log(\sqrt{S_{ij}S_{ij}} \times \delta_{th}/S_L)$ at the central mid-plane is shown in Figs. 1(a)–1(c) for cases A–C, respectively, and the contours of $c_T = 0.15,\ 0.3,\ 0.5,\ 0.7$, and 0.85 (left to right) are superimposed on top of it. The distributions of $\sqrt{S_{ij}S_{ij}}$ in cases A–C are markedly different. In case A, occasional local augmentations of $\sqrt{S_{ij}S_{ij}}$ from the unburned to the burned gas side of the flame front can be discerned, whereas the strain rate magnitude drops significantly from the unburned to the burned gas side of the flame front in cases B and C. Moreover, the strain rate magnitudes change significantly in a short span of space in the unburned gas region in cases B and C, whereas the length scale associated with the variation of $\sqrt{S_{ij}S_{ij}}$ in case A is much greater than in cases B and C.

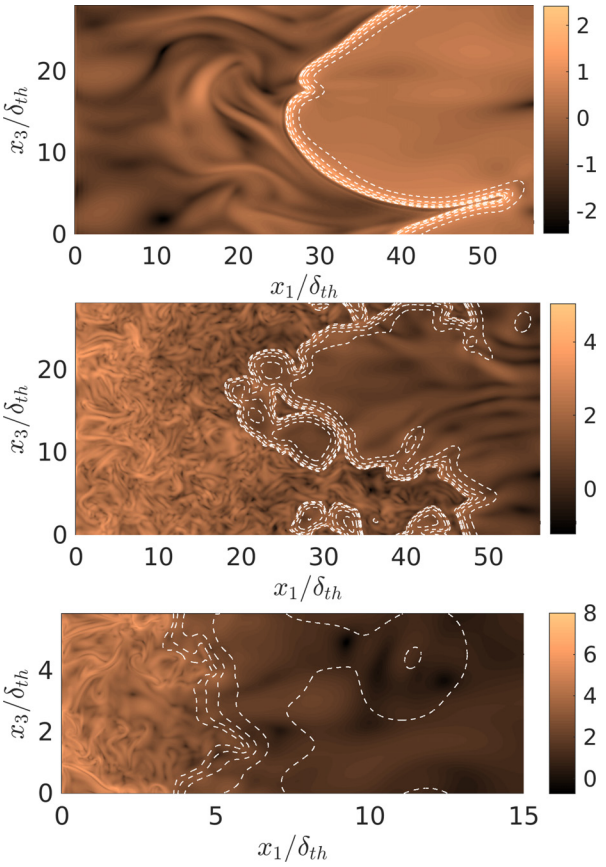

FIG. 1. Distributions of $\log(\sqrt{S_{ij}S_{ij}} \times \delta_{th}/S_L)$ in the central midplane for (a)–(c) cases A–C (note the different scale for case C). The white broken lines indicate $c = 0.15,\ 0.3,\ 0.5,\ 0.7$, and 0.85 from left to right.

It is worthwhile to note that cases B and C have higher values of Re_t than in case A, and thus, they exhibit a larger range of length scales than in case A. Note that l_T is identical in cases A and B, but the Kolmogorov length scale $\eta \sim l_T Re_t^{-3/4}$ is smaller in case B than in case A because of the higher Re_t value in case B. Moreover, l_T in case C is smaller than that in case A, and thus, the Kolmogorov length scale $\eta \sim l_T Re_t^{-3/4}$ in case C is smaller than in case A due to the much higher Re_t value in case C. As the Karlovitz number Ka scales as $Ka \sim \delta_{th}^2/\eta^2$,[29] the flame thickness δ_{th} remains smaller than the Kolmogorov length scale η in case A (where $Ka < 1$), but $\delta_{th} > \eta$ is obtained for cases B and C. Thus, the scale separation between δ_{th} and

TABLE I. List of inflow turbulence parameters.

Case	u'/S_L	l_T/δ_{th}	Re_t	Da	Ka
A	0.7	14.0	227	20.0	0.75
B	5.0	14.0	1623	2.8	14.4
C	14.0	4.0	1298	0.29	126

η is greater in case C than in case B due to the greater Ka value for case C. As a result, the inner flame structure in cases B and C gets affected by turbulent fluctuations, and this is reflected in the local flame thickening in these cases, which can, indeed, be verified from the lack of the parallel nature of the contours of c_T in Figs. 1(b) and 1(c). By contrast, the contours of c_T remain parallel to each other in case A as the inner flame structure is not affected by turbulent fluid motion in this case. From the foregoing discussion, it can be appreciated that the strain rate distribution and the flame–turbulence interaction are significantly affected by the Karlovitz number, which will be reflected in the alignment statistics of pressure Hessian eigenvectors with strain rate eigenvectors and reaction scalar gradient (or flame normal vector $\boldsymbol{N}$).

The mean values of normalized principal strain rates $\{s_\alpha, s_\beta, s_\gamma\} \times \delta_{th}/S_L$ (with $s_\alpha > s_\beta > s_\gamma$) conditional upon c_T are shown in Figs. 2(a)–2(c) for cases A–C, respectively, along with the mean normalized dilatation rate $\nabla \cdot \mathbf{u} \times \delta_{th}/S_L = \{s_\alpha + s_\beta + s_\gamma\} \times \delta_{th}/S_L$. It is evident from Fig. 2 that the individual principal strain rates tend to increase from case A to case C, which is consistent with the observations made from Figs. 1(a)–1(c). However, the magnitudes of $\nabla \cdot \mathbf{u}$ remain comparable. Figures 2(a)–2(c) also show that the peak mean value of $\nabla \cdot \mathbf{u}$ is obtained for $0.2 < c_T < 0.4$ for all cases because the effects of heat release are strong in this region of the flame for H_2–air flames with $\phi = 0.7$, for which the maximum heat release rate occurs at $c_T \approx 0.3$ under laminar conditions. Figures 2(a)–2(c) further reveal that the magnitude of the most extensive principal strain rate s_α remains greater than the magnitudes of the intermediate and the most compressive principal strain rates (i.e., s_β and s_γ) in case A, whereas the mean values of s_α and s_γ are of similar magnitude in case C, and the behavior in case B is somewhere in between cases A and C. This suggests that the preferential augmentation of the magnitude of s_α weakens with increasing (decreasing) Ka (Da) (i.e., from cases A and C), and this behavior affects the statistics of the scalar–turbulence interaction term $\overline{\rho}\tilde{\Delta}_c$, which can be expressed as[18,21]

$$\overline{\rho}\tilde{\Delta}_c = \overline{2\rho D_c |\nabla c|^2 \left[s_\alpha \cos^2(\hat{e}_\alpha, \boldsymbol{N} + s_\beta \cos^2(\hat{e}_\beta, \boldsymbol{N}) + s_\gamma \cos^2(\hat{e}_\gamma, \boldsymbol{N})\right]}. \tag{5}$$

Equation (5) suggests that a preferential alignment between $\boldsymbol{N}$ and $\hat{e}_\alpha$ ($\hat{e}_\gamma$) yields a positive (negative) value of Δ_c, which is indicative of destruction (generation) of the reactive scalar gradient by flame normal straining.[18,21]

The relative alignment of $\boldsymbol{N}$ and $\hat{e}_i$ (with $i = \alpha, \beta,$ and γ) can be quantified by $\Gamma_\alpha = |\cos(\boldsymbol{N}, \hat{e}_\alpha)|$, $\Gamma_\beta = |\cos(\boldsymbol{N}, \hat{e}_\beta)|$, and $\Gamma_\gamma = |\cos(\boldsymbol{N}, \hat{e}_\gamma)|$, so that a unity value of these quantities (i.e., $\Gamma_i = \cos 0^\circ = 1$ for $i = \alpha, \beta,$ and γ) signifies a perfect collinear alignment, whereas a zero value (i.e., $\Gamma_i = \cos 90^\circ = 0$ for $i = \alpha, \beta,$ and γ) represents a perpendicular alignment. The mean values of Γ_α, Γ_β, and Γ_γ conditional upon c_T are shown in Figs. 3(a)–3(c) for cases A–C, respectively, for c based on H_2 mass fraction, but the same qualitative behavior has been observed for reaction progress variables using O_2 and H_2O mass fractions. It is seen from Figs. 3(a)–3(c) that the flame normal vector $\boldsymbol{N}$ preferentially aligns collinearly with $\hat{e}_\alpha$ in case A for most of the flame front except for the burned gas side, where an increase in the collinear alignment between $\boldsymbol{N}$ and $\hat{e}_\gamma$ is observed. In case C, $\boldsymbol{N}$ exhibits a predominant collinear alignment with $\hat{e}_\gamma$ for a major part of the flame, but an increase in the collinear alignment between $\boldsymbol{N}$ and $\hat{e}_\alpha$ is observed in the burned gas region. In case B, $\boldsymbol{N}$ also collinearly aligns with $\hat{e}_\alpha$, but the extent of this alignment is weaker (stronger) than in case A (case C). In contrast, the extent of collinear alignment of $\boldsymbol{N}$ with $\hat{e}_\gamma$ in case B is stronger (weaker) than in case A (case C). It has been shown elsewhere[3,21] that $\boldsymbol{N}$ (or ∇c)

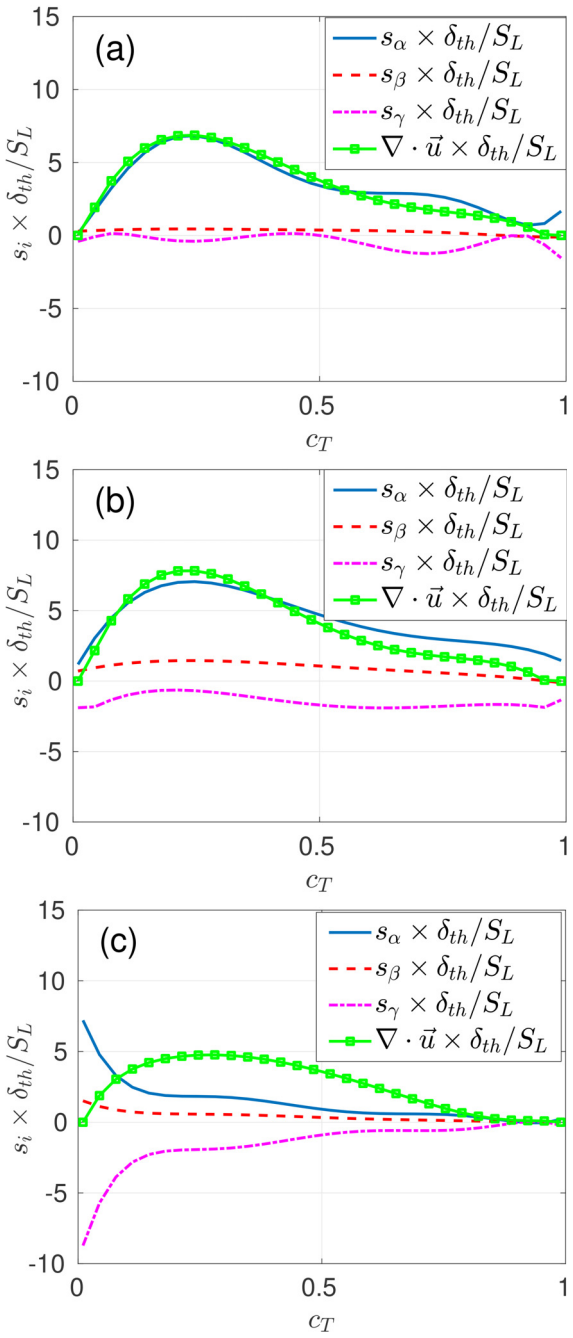

FIG. 2. Profiles of mean values of $\{s_\alpha, s_\beta, s_\gamma,$ and $\nabla \cdot \vec{u}\} \times \delta_{th}/S_L$ (with $s_\alpha > s_\beta > s_\gamma$) conditional upon c_T for (a)–(c) cases A–C. Note that s_α, s_β, and s_γ are multiplied by 0.1 in case C.

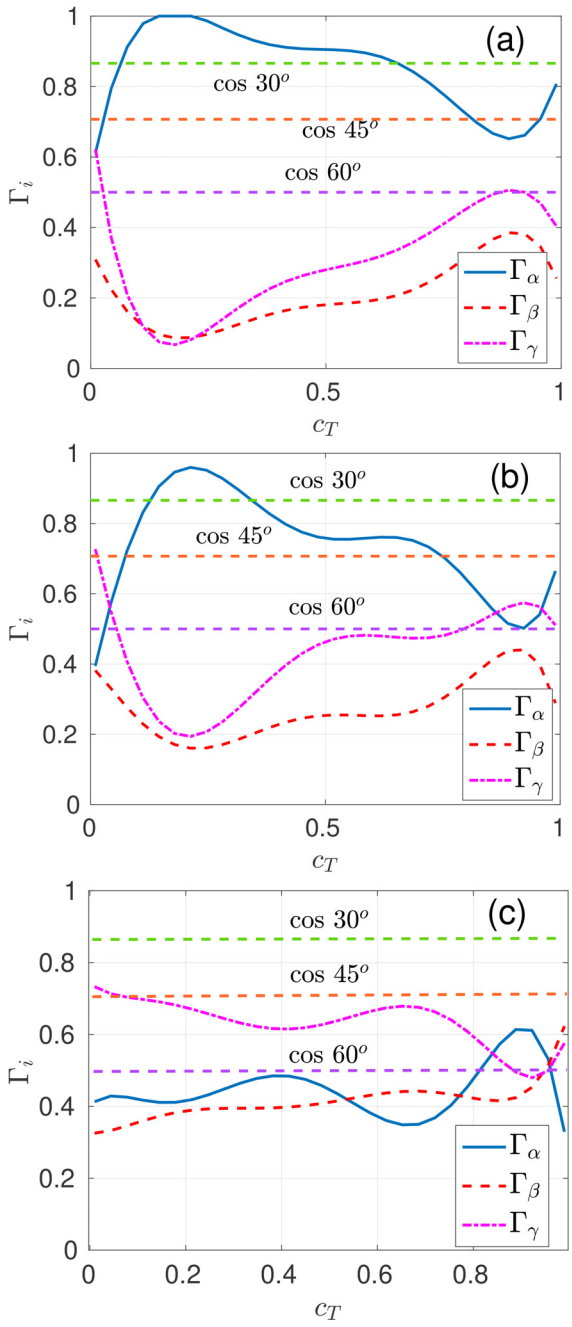

FIG. 3. Profiles of mean values of Γ_α (blue solid), Γ_β (red broken), and Γ_γ (magenta chain dotted) conditional upon c_T for (a)–(c) cases A–C. $\mathbf{N}$ is calculated based on c definition based on H_2 mass fraction in Figs. 3 and 4. Horizontal green, orange, and purple lines indicate $\cos 30^\circ$, $\cos 45^\circ$, and $\cos 60^\circ$, respectively, in Figs. 3–7.

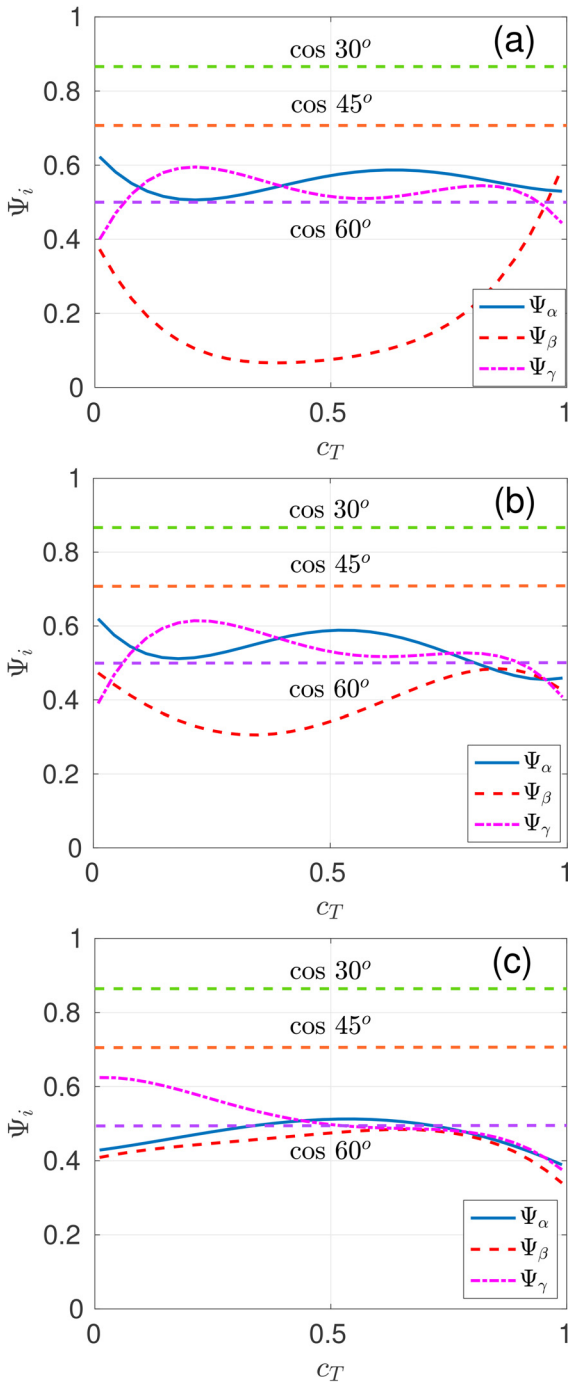

FIG. 4. Profiles of mean values of Ψ_α (blue solid), Ψ_β (red broken), and Ψ_γ (magenta chain dotted) conditional upon c_T for (a)–(c) cases A–C.

preferentially aligns with $\hat{e}_\alpha$ for $(T_{ad} - T_0)Da_l/T_0 \gg 1$ (where $Da_l = L_{11}S_L/\delta_{th}u'$ is the Damköhler number based on the longitudinal integral length scale L_{11}), which signifies that the strain rate induced by flame normal acceleration arising from thermal expansion overwhelms turbulent straining. On the contrary, $\boldsymbol{N}$ (or ∇c) preferentially aligns with $\hat{e}_\gamma$ similar to non-reacting flows, for $(T_{ad} - T_0)Da_l/T_0 \ll 1$ when turbulent straining dominates over the strain rate due to thermal expansion. The values of $(T_{ad} - T_0)Da_l/T_0$

are 45.68, 6.40, and 0.66 in cases A, B, and C, respectively, and thus, $\boldsymbol{N}$ (or ∇c) predominantly aligns with $\hat{e}_\alpha$ ($\hat{e}_\gamma$) in cases A and B (case C).

Based on the above information, it will be useful to consider the relative alignment between $\boldsymbol{N}$ and $\hat{\pi}_i$ (for $i = \alpha, \beta,$ and γ) in order to understand how the pressure Hessian contribution (i.e., F_{12}) affects the evolution of $\overline{\rho}\tilde{\Delta}_c$ within the flame front [see Eqs. (2) and (4)]. Based on the close relation of the pressure Hessian $\boldsymbol{\Pi}$ with the evolutions of $\tilde{\Delta}_c$ and s_i (for $i = \alpha, \beta,$ and γ), the alignments of $\hat{\pi}_i$ (for $i = \alpha, \beta,$ and γ) with $\boldsymbol{N}$ and with $\hat{e}_i$ (for $i = \alpha, \beta,$ and γ) will be analyzed next.

The mean values of $\Psi_\alpha = |\cos(\boldsymbol{N}, \hat{\pi}_\alpha)|$, $\Psi_\beta = |\cos(\boldsymbol{N}, \hat{\pi}_\beta)|$, and $\Psi_\gamma = |\cos(\boldsymbol{N}, \hat{\pi}_\gamma)|$ conditional upon c_T are shown in Figs. 4(a)–4(c) for cases A–C, respectively, where $\boldsymbol{N}$ is evaluated based on c using H_2 mass fraction, but the same qualitative behavior has been observed for c definitions using O_2 and H_2O mass fractions (not shown here). Figures 4(a) and 4(b) suggest that the mean values of Ψ_α and Ψ_γ conditional upon c_T remain comparable, and both remain greater than the mean value of Ψ_β in cases A and B. In contrast, the mean value of Ψ_γ assumes greater values than that of Ψ_α and Ψ_β toward the unburned gas side ($c_T < 0.4$) in case C. Figures 4(a)–4(c) indicate that the mean values of Ψ_α, Ψ_β, and Ψ_γ are sufficiently different from unity, suggesting that $\hat{\pi}_\alpha$ and $\hat{\pi}_\gamma$ remain in imperfect alignment with $\boldsymbol{N}$ (and ∇c), and $\hat{\pi}_\beta$ does not collinearly align with $\boldsymbol{N}$ (and ∇c) in all cases considered here.

The pressure gradient ∇p remains imperfectly aligned with $\mathbf{N}$ for high values of u'/S_L such as in cases B and C (not shown here), whereas ∇p aligns with $\boldsymbol{N}$ for small values of u'/S_L (e.g., case A) similar to that in laminar flames. As shown in Fig. 3, $\boldsymbol{N}$ preferentially collinearly aligns with $\hat{e}_\alpha$ in case A, and also in the region of intense heat release in case B, whereas a predominant alignment between $\boldsymbol{N}$ and $\hat{e}_\gamma$ is obtained in case C. Therefore, it is of interest to consider the relative alignments between $\hat{\pi}_i$ (for $i = \alpha, \beta,$ and γ) and $\hat{e}_k$ (for $k = \alpha, \beta,$ and γ).

The mean values of $\Phi_{ij} = |\cos(\hat{\pi}_i, \hat{e}_j)|$ (for $i = \alpha, \beta,$ and γ and $j = \alpha, \beta,$ and γ) conditional upon c_T are shown in Fig. 5 for case A. The corresponding variations for cases B and C are shown in Figs. 6 and 7, respectively. Figure 5(a) shows that the mean value of $\Phi_{\alpha\alpha}$ ($\Phi_{\alpha\beta}$) assumes the highest (smallest) value among the mean values of $\Phi_{\alpha\alpha}, \Phi_{\alpha\beta}$, and $\Phi_{\alpha\gamma}$ in case A. However, all of these mean values remain comparable and smaller than $\cos 45^\circ = 0.707$, suggesting an imperfect alignment of $\hat{\pi}_\alpha$ for all strain rate eigenvectors $\hat{e}_\alpha, \hat{e}_\beta$, and $\hat{e}_\gamma$. A comparison between Figs. 5(a) and 5(c) reveals that the profiles of the mean values of $\Phi_{\gamma\alpha}, \Phi_{\gamma\beta}$, and $\Phi_{\gamma\gamma}$ remain qualitatively similar to that of $\Phi_{\alpha\alpha}, \Phi_{\alpha\beta}$, and $\Phi_{\alpha\gamma}$, respectively, which also suggests an imperfect alignment of $\hat{\pi}_\gamma$ with $\hat{e}_\alpha, \hat{e}_\beta$, and $\hat{e}_\gamma$. In contrast, the mean values of $\Phi_{\beta\beta}$ and $\Phi_{\beta\gamma}$ remain greater than that of $\Phi_{\beta\alpha}$ and assume values close to 0.6 throughout the flame front, suggesting an imperfect alignment of $\hat{\pi}_\beta$ with $\hat{e}_\beta$ and $\hat{e}_\gamma$, and a very little alignment between $\hat{\pi}_\beta$ with $\hat{e}_\alpha$. Under homogeneous isotropic non-reacting turbulent flows, $\hat{\pi}_\beta$ has a tendency to align collinearly with $\hat{e}_\beta$,[11,13] whereas in homogeneous axisymmetric non-reacting flows, $\hat{\pi}_\gamma$ preferentially aligns, collinearly with $\hat{e}_\beta$.[14] Figure 5 suggests that the presence of heat release in case A alters the collinear alignment of $\hat{e}_\beta$ with either $\hat{\pi}_\beta$ or $\hat{\pi}_\gamma$.

It was demonstrated earlier[3,21] that the strength of the strain rate induced by thermal expansion in comparison to turbulent straining processes weakens with increasing (decreasing) Ka (Da), and the same is also valid for this database (i.e., from case A to case C).[3,21] Thus, the

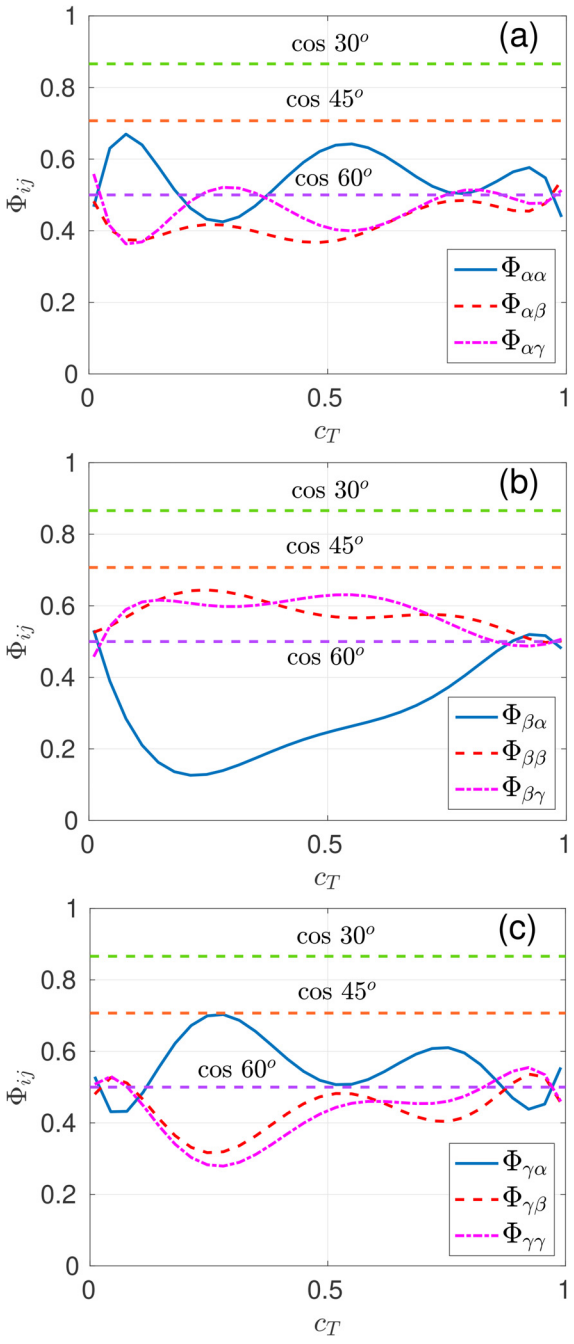

FIG. 5. Profiles of mean values of (a) $\Phi_{\alpha\alpha}$ (blue solid), $\Phi_{\alpha\beta}$ (red broken), and $\Phi_{\alpha\gamma}$ (magenta chain dotted); (b) $\Phi_{\beta\alpha}$ (blue solid), $\Phi_{\beta\beta}$ (red broken), and $\Phi_{\beta\gamma}$ (magenta chain dotted); and (c) $\Phi_{\gamma\alpha}$ (blue solid), $\Phi_{\gamma\beta}$ (red broken), and $\Phi_{\gamma\gamma}$ (magenta chain dotted) conditional upon c_T for case A.

alignments between $\hat{\pi}_i$ (for $i = \alpha, \beta,$ and γ) and $\hat{e}_j$ (for $j = \alpha, \beta,$ and γ) change from case A to case C. In case B, the mean values of $\Phi_{\alpha\alpha}, \Phi_{\alpha\beta}$, and $\Phi_{\alpha\gamma}$ assume comparable values [see Fig. 6(a)], and the mean values of $\Phi_{\beta\alpha}$ and $\Phi_{\gamma\alpha}$ remain the highest among

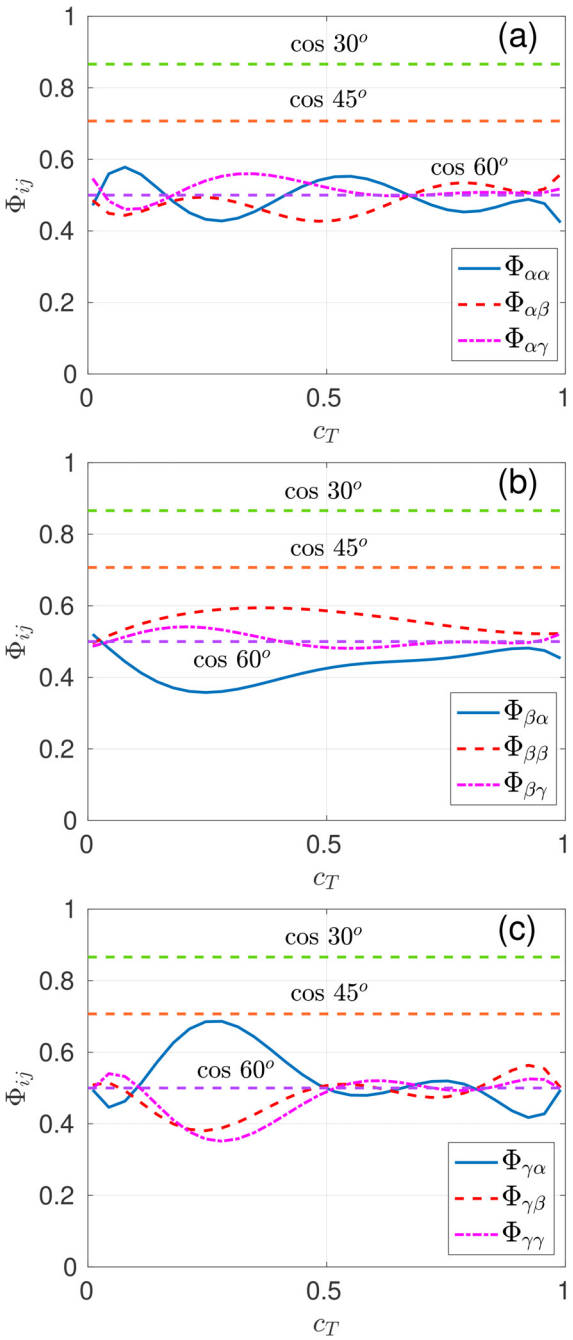

FIG. 6. Profiles of mean values of (a) $\Phi_{\alpha\alpha}$ (blue solid), $\Phi_{\alpha\beta}$ (red broken), and $\Phi_{\alpha\gamma}$ (magenta chain dotted); (b) $\Phi_{\beta\alpha}$ (blue solid), $\Phi_{\beta\beta}$ (red broken), and $\Phi_{\beta\gamma}$ (magenta chain dotted); and (c) $\Phi_{\gamma\alpha}$ (blue solid), $\Phi_{\gamma\beta}$ (red broken), and $\Phi_{\gamma\gamma}$ (magenta chain dotted) conditional upon c_T for case B.

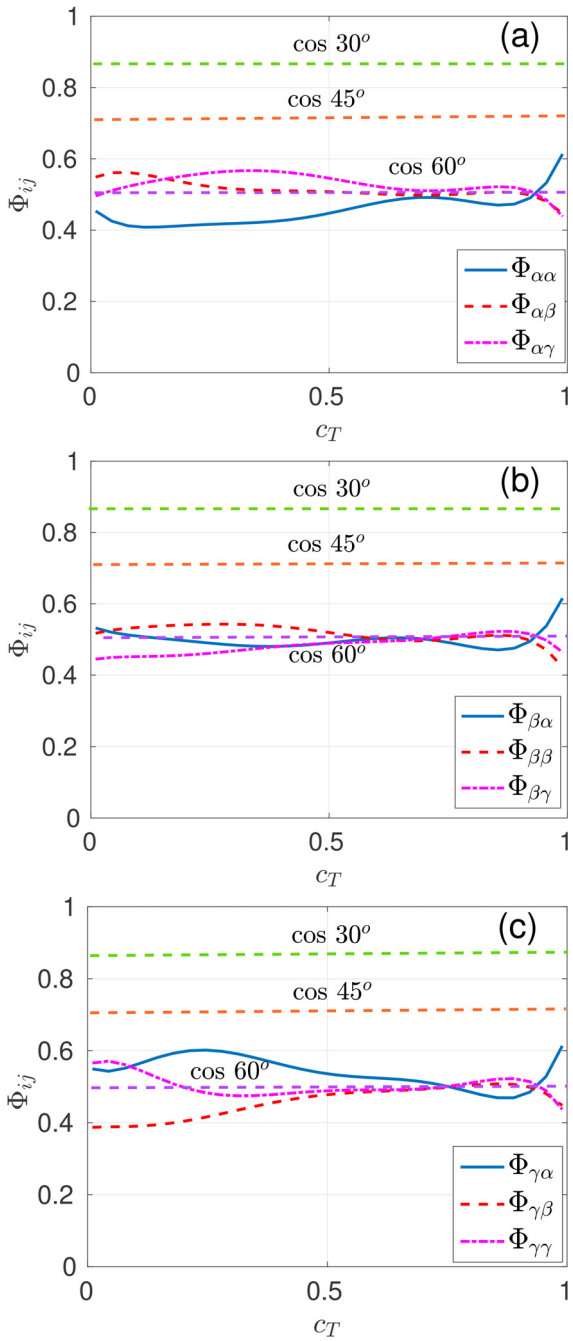

FIG. 7. Profiles of mean values of (a) $\Phi_{\alpha\alpha}$ (blue solid), $\Phi_{\alpha\beta}$ (red broken), and $\Phi_{\alpha\gamma}$ (magenta chain dotted); (b) $\Phi_{\beta\alpha}$ (blue solid), $\Phi_{\beta\beta}$ (red broken), and $\Phi_{\beta\gamma}$ (magenta chain dotted); and (c) $\Phi_{\gamma\alpha}$ (blue solid), $\Phi_{\gamma\beta}$ (red broken), and $\Phi_{\gamma\gamma}$ (magenta chain dotted) conditional upon c_T for case C.

$\Phi_{\beta\alpha}, \Phi_{\beta\beta}$, and $\Phi_{\beta\gamma}$ and $\Phi_{\gamma\alpha}, \Phi_{\gamma\beta}$, and $\Phi_{\gamma\gamma}$, respectively [see Figs. 6(b) and 6(c)]. The mean value of $\Phi_{\beta\alpha}$ is the smallest among $\Phi_{\beta\alpha}, \Phi_{\beta\beta}$, and $\Phi_{\beta\gamma}$ in case B, which is qualitatively similar to case A. This indicates that heat release effects in case B induce a misalignment between pressure Hessian (i.e., $\hat{\pi}_i$ for $i = \alpha, \beta,$ and γ) and strain rate eigenvectors (i.e., $\hat{e}_j$ for $j = \alpha, \beta,$ and γ). The alignment statistics between pressure Hessian eigenvectors (i.e., $\hat{\pi}_i$ for $i = \alpha, \beta,$ and γ) and strain rate

eigenvectors (i.e., $\hat{e}_j$ for $j = \alpha, \beta,$ and γ) in cases A and B is consistent with previous findings based on simple chemistry DNS data.[16]

A comparison among Figs. 5–7 reveals that the alignment statistics between $\hat{\pi}_\alpha$ and strain rate eigenvectors (i.e., $\hat{e}_j$ for $j = \alpha, \beta,$ and γ) in case C is significantly different from that in cases A and B [see Figs. 5(a), 6(a), and 7(a)]. In case C, the mean values of $\Phi_{\alpha\beta}$ and $\Phi_{\alpha\gamma}$ remain greater than the mean value of $\Phi_{\alpha\alpha}$ for a major part of the flame front except for the burned gas side of the flame. The mean value of $\Phi_{\beta\beta}$ remains the cosine magnitude with the highest value for a major part of the flame front except for the burned gas side among $\Phi_{\beta\alpha}$, $\Phi_{\beta\beta}$, and $\Phi_{\beta\gamma}$ in case C, but their values remain comparable. The mean value of $\Phi_{\beta\beta}$ in case C is smaller than that obtained in cases A and B. The mean value of $\Phi_{\gamma\alpha}$ remains the highest among $\Phi_{\gamma\alpha}$, $\Phi_{\gamma\beta}$, and $\Phi_{\gamma\gamma}$ in case C, which is qualitatively similar to the behavior observed for cases A and B [see Figs. 5(c), 6(c), and 7(c)]. The observations from Fig. 7 also indicate that the heat release effects within the high Karlovitz number flames remain strong enough to exhibit differences from the predominant alignment between $\hat{\pi}_\beta$ ($\hat{\pi}_\gamma$) and $\hat{e}_\beta$ in homogeneous isotropic (axisymmetric) non-reacting turbulence.[11,13,14] The imperfect alignments between $\hat{\pi}_i$ (i.e., $\hat{\pi}_i$ for $i = \alpha, \beta,$ and γ) and strain rate eigenvectors (i.e., $\hat{e}_j$ for $j = \alpha, \beta,$ and γ) and comparable values of $\Phi_{\alpha\alpha}$, $\Phi_{\beta\alpha}$, and $\Phi_{\gamma\alpha}$ ($\Phi_{\alpha\beta}$, $\Phi_{\beta\beta}$, and $\Phi_{\gamma\beta}$) [$\Phi_{\alpha\gamma}$, $\Phi_{\beta\gamma}$, and $\Phi_{\gamma\gamma}$] reveal that $\hat{\Pi}_\alpha$ ($\hat{\Pi}_\beta$) [$\hat{\Pi}_\gamma$] is determined by the eigenvalues of the pressure Hessian (i.e., $\Pi_\alpha, \Pi_\beta,$ and Π_γ) according to Eq. (3). Similarly, comparable values of Ψ_α and Ψ_γ indicate that the behavior of F_{12} is driven by the relative magnitudes of Π_α and Π_γ [see Eq. (4)]. It has been found that the mean values of Ψ_α remain comparable to that of Ψ_γ for a major part of the flame front in cases A–C [see Figs. 4(a)–4(c)], and the mean value of the trace of pressure Hessian ($\Pi_\alpha + \Pi_\beta + \Pi_\gamma$) is determined by the mean value of ($\Pi_\alpha + \Pi_\gamma$) (not shown here). The mean values of $\{\hat{\Pi}_N = (\Pi_\alpha \cos^2\Psi_\alpha + \Pi_\beta \cos^2\Psi_\beta + \Pi_\gamma \cos^2\Psi_\gamma),\ \hat{\Pi}_\alpha,\ \hat{\Pi}_\beta,\ \hat{\Pi}_\gamma\} \times \delta_{th}^2/\rho_0 S_L^2$ conditional upon c_T for cases A–C are shown in Figs. 8(a)–8(c), respectively.

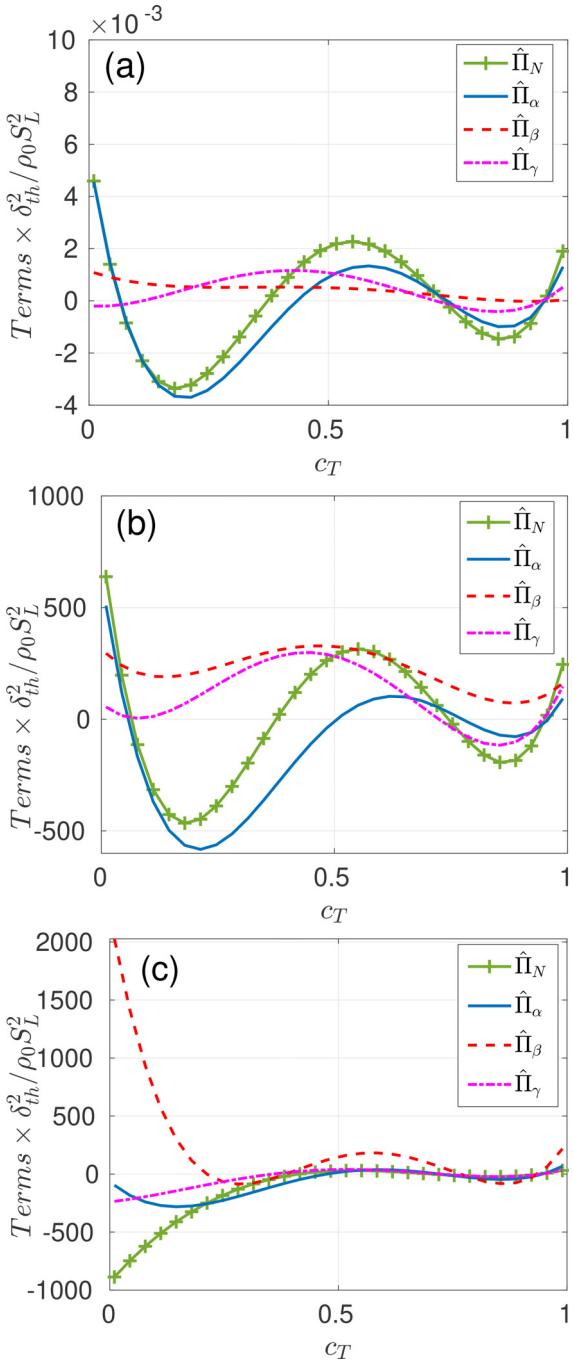

FIG. 8. Profiles of the mean values of $\{\hat{\Pi}_N, \hat{\Pi}_\alpha, \hat{\Pi}_\beta, \hat{\Pi}_\gamma\} \times \delta_{th}^2/\rho_0 S_L^2$ conditional upon c_T for (a)–(c) cases A–C.

Figures 8(a)–8(c) show that the mean value of $\hat{\Pi}_N$ assumes negative values for $0.1 < c_T < 0.4$ where the effects of the dilatation rate are the strongest (see Fig. 2). Equation (4) suggests that a negative value of $\hat{\Pi}_N$ tends to induce positive values of F_{12}, which acts to increase the positive value of $\tilde{\Delta}_c$ [see Eq. (2)], indicating an increased (a reduced) extent of collinear alignment between $\hat{e}_\alpha$ ($\hat{e}_\gamma$) and $\boldsymbol{N}$. Figure 8 also demonstrates that $\hat{\Pi}_\alpha$ assumes the highest magnitude among the quantities $\hat{\Pi}_\alpha$, $\hat{\Pi}_\beta$, and $\hat{\Pi}_\gamma$ in cases A and B, indicating that $\boldsymbol{\Pi}$ influences particularly the evolution of s_α in these cases. Furthermore, Eqs. (1) and (3) suggest that the predominantly negative values of $\hat{\Pi}_\alpha$ act to increase s_α in cases A and B, but both s_β and s_γ in these cases are not severely affected by the pressure Hessian due to small magnitudes of $\hat{\Pi}_\beta$ and $\hat{\Pi}_\gamma$ in comparison to $\hat{\Pi}_\alpha$. However, $\hat{\Pi}_\beta$ assumes the highest magnitude among the quantities $\hat{\Pi}_\alpha$, $\hat{\Pi}_\beta$, and $\hat{\Pi}_\gamma$ in case C, and thus, the pressure Hessian does not significantly influence the evolutions of s_α and s_γ. However, the mean value of $\hat{\Pi}_\alpha$ remains predominantly negative in case C and, therefore, acts to increase s_α, but the influences of $\boldsymbol{\Pi}$ on s_α and s_γ weaken with increasing Ka (i.e., from case A to case C). The above findings suggest that the influence of pressure Hessian could be important for flames with small (large) values of Ka (Da), which is consistent with recent findings by Kasten *et al.*[16] in the context of simple chemistry DNS and experimental findings by Steinberg *et al.*[15] The current analysis suggests that $\boldsymbol{\Pi}$ may play a key role in the alteration of ∇c (or $\vec{N}$) alignment with strain rate eigenvectors in high Da and low Ka turbulent premixed flames in comparison to that in the case of passive scalar mixing, as previously conjectured by Gonzalez and Paranthoën.[19,20]

IV. CONCLUSIONS

The alignment statistics of the eigenvectors of pressure Hessian $\mathbf{\Pi}$ with ∇c and strain rate eigenvectors in turbulent premixed flames has been analyzed for *Ka* (*Da*) values ranging from 0.75 to 126 (0.29 to 20.0) using a detailed chemistry three-dimensional DNS database of fuel-lean H_2–air premixed flames with $\phi = 0.7$. It was found that ∇c preferentially aligns with the eigenvector corresponding to the most extensive principal strain rate with large *Da* and small *Ka*, but the reactive scalar gradient in flames with small *Da* and large *Ka* exhibits a preferential collinear alignment with the eigenvector corresponding to the most compressive principal strain rate. It was also found that the eigenvectors of $\mathbf{\Pi}$ exhibit imperfect alignment with ∇c. However, the net contribution of the pressure Hessian to the evolution of the scalar–turbulence interaction term (i.e., normal strain rate contribution to the scalar dissipation rate transport) in the zone of high dilatation rate acts to increase the normal strain rate and, thus, to reduce $|\nabla c|$. Moreover, the relative collinear alignments of $\mathbf{\Pi}$ and strain rate eigenvectors have been found to be different from those in the non-reacting turbulent flows. Furthermore, the relative alignments of the eigenvectors of $\mathbf{\Pi}$ and the strain rate are such that the contribution of $\mathbf{\Pi}$ to the evolution of principal strain rates tends to augment the most extensive principal strain rate for small and moderate values of *Ka*, but this behavior weakens for $Ka \sim 100$ where the contribution of $\mathbf{\Pi}$ plays an important role for the evolution of the intermediate principal strain rate.

The findings of the current analysis suggest that the contributions of $\mathbf{\Pi}$ to the evolution of scalar–turbulence interaction and principal strain rates weaken with increasing the Karlovitz number, but these effects might play significant roles for small and moderate values of *Ka*. The results further indicate that the contributions of $\mathbf{\Pi}$ might be pivotal to the alteration of ∇c alignment with strain rate eigenvectors in comparison to that in the case of passive scalar mixing in turbulent premixed flames with high *Da* and low *Ka*, as conjectured previously based on analytical studies[19,20] on inviscid flows.

ACKNOWLEDGMENTS

N.C. and U.A. are grateful to EPSRC and ARCHER (No. EP/R029369/1) for computational support. H.G.I. is grateful to KAUST for research funding and computational support.

AUTHOR DECLARATIONS

Conflict of Interest

The authors have no conflicts to disclose.

Author Contributions

Nilanjan Chakraborty: Conceptualization (lead); Formal analysis (lead); Funding acquisition (lead); Project administration (lead); Software (lead); Supervision (lead); Writing – original draft (lead); Writing – review & editing (lead). **Umair Ahmed:** Conceptualization (supporting); Formal analysis (equal); Writing – review & editing (supporting). **Markus Klein:** Formal analysis (supporting); Writing – review & editing (supporting). **Hong G. Im:** Funding acquisition (lead); Project administration (supporting); Resources (lead); Writing – review & editing (supporting).

DATA AVAILABILITY

The data that support the findings of this study are available from the corresponding author upon reasonable request.

REFERENCES

[1]R. Borghi and D. Escudie, "Assessment of a theoretical model of turbulent combustion by comparison with a simple experiment," Combust. Flame **56**, 149–164 (1984).
[2]D. Veynante and T. Poinsot, "Effects of pressure gradient in turbulent premixed flames," J. Fluid Mech. **353**, 83–114 (1997).
[3]N. Chakraborty, "Influence of thermal expansion on fluid dynamics of turbulent premixed combustion and its modelling implications," Flow, Turbul. Combust. **106**, 753–848 (2021).
[4]S. Zhang and C. J. Rutland, "Premixed flame effects on turbulence and pressure-related terms," Combust. Flame **102**, 447–461 (1995).
[5]S. Nishiki, T. Hasegawa, R. Borghi, and R. Himeno, "Modeling of flame-generated turbulence based on direct numerical simulation databases," Proc. Combust. Inst. **29**, 2017–2022 (2002).
[6]N. Chakraborty, M. Katragadda, and R. S. Cant, "Statistics and modelling of turbulent kinetic energy transport in different regimes of premixed combustion," Flow, Turbul. Combust. **87**, 205–235 (2011).
[7]A. N. Lipatnikov, S. Nishiki, and T. Hasegawa, "A direct numerical study of vorticity transformation in weakly turbulent premixed flames," Phys. Fluids **26**, 105104 (2014).
[8]N. Chakraborty, I. Konstantinou, and A. Lipatnikov, "Effects of Lewis number on vorticity and enstrophy transport in turbulent premixed flames," Phys. Fluids **28**, 015109 (2016).
[9]C. Dopazo, L. Cifuentes, and N. Chakraborty, "Vorticity budgets in premixed combusting turbulent flows at different Lewis numbers," Phys. Fluids **29**, 045106 (2017).
[10]V. Papapostolou, D. H. Wacks, M. Klein, N. Chakraborty, and H. G. Im, "Enstrophy transport conditional on local flow topologies in different regimes of premixed turbulent combustion," Sci. Rep. **7**, 11545 (2017).
[11]C. Kalelkar, "Statistics of pressure fluctuations in decaying isotropic turbulence," Phys. Rev. E **73**, 046301 (2006).
[12]B. Lüthi, M. Holzner, and A. Tsinober, "Expanding the Q-R space to three dimensions," J. Fluid Mech. **641**, 497–507 (2009).
[13]S. Suman and S. S. Girimaji, "Velocity gradient dynamics in compressible turbulence: Characterization of pressure-Hessian tensor," Phys. Fluids **25**(12), 125103 (2013).
[14]J. M. Lawson and J. R. Dawson, "On velocity gradient dynamics and turbulent structure," J. Fluid Mech. **780**, 60–98 (2015).
[15]A. M. Steinberg, B. Coriton, and J. H. Frank, "Influence of combustion on principal strain-rate transport in turbulent premixed flames," Proc. Combust. Inst. **35**, 1287–1296 (2015).
[16]C. Kasten, U. Ahmed, M. Klein, and N. Chakraborty, "Principal strain rate evolution within turbulent premixed flames for different combustion regimes," Phys. Fluids **33**, 015111 (2021).
[17]U. Ahmed, R. Prosser, and A. J. Revell, "Towards the development of an evolution equation for flame turbulence interaction in premixed turbulent combustion," Flow, Turbul. Combust. **93**, 637–663 (2014).
[18]U. Ahmed and R. Prosser, "Modelling flame turbulence interaction in RANS simulation of premixed turbulent combustion," Combust. Theory Modell. **20**, 34–57 (2016).
[19]M. Gonzalez and P. Paranthoën, "Effect of density step on stirring properties of a strain flow," Fluid Dyn. Res. **41**, 035508 (2009).
[20]M. Gonzalez and P. Paranthoën, "Effect of variable mass density on the kinematics of scalar gradient," Phys. Fluids **23**, 075107 (2011).
[21]N. Chakraborty and N. Swaminathan, "Influence of Damköhler number on turbulence-scalar interaction in premixed flames. Part I: Physical insight," Phys. Fluids **19**, 045103 (2007).
[22]C. Keylock, "The Schur decomposition of the velocity gradient tensor for turbulent flows," J. Fluid Mech. **848**, 876–905 (2018).
[23]H. G. Im, P. G. Arias, S. Chaudhuri, and H. A. Uranakara, "Direct numerical simulations of statistically stationary turbulent premixed flames," Combust. Sci. Technol. **188**, 1182–1198 (2016).

[24]M. P. Burke, M. Chaos, Y. Ju, F. L. Dryer, and S. J. Klippenstein, "Comprehensive H_2-O_2 kinetic model for high-pressure combustion," Int. J. Chem. Kinet. **44**, 444–474 (2012).
[25]J. H. Chen and H. G. Im, "Stretch effects on the burning velocity of turbulent premixed hydrogen/air flames," Proc. Combust. Inst. **28**, 211–218 (2000).
[26]H. G. Im and J. H. Chen, "Preferential diffusion effects on the burning rate of interacting turbulent premixed hydrogen-air flames," Combust. Flame **131**, 246–258 (2002).
[27]I. Han and K. Y. Huh, "Effects of the Karlovitz number on the evolution of the flame surface density in turbulent premixed flames," Combust. Flame **152**, 194–205 (2008).
[28]C. Dopazo, L. Cifuentes, J. Martin, and C. Jimenez, "Strain rates normal to approaching iso-scalar surfaces in a turbulent premixed flame," Combust. Flame **162**, 1729–1736 (2015).
[29]N. Peters, *Turbulent Combustion* (Cambridge University Press, 2000).
[30]T. Poinsot and D. Veynante, *Theoretical and Numerical Combustion* (R.T. Edwards Inc., Philadelphia, 2001).
[31]T. Falkenstein, S. Kang, L. Cai, M. Bode, and H. Pitsch, "DNS study of the global heat release rate during early flame kernel development under engine conditions," Combust. Flame **213**, 455–466 (2020).
[32]X. Wang, "Direct numerical simulation of lean premixed turbulent flames at high Karlovitz numbers under elevated pressures," Ph.D. thesis (University College London, London, 2019).
[33]E. Inanc, A. M. Kempf, and N. Chakraborty, "Scalar gradient and flame propagation statistics of a flame-resolved laboratory-scale turbulent stratified burner simulation," Combust. Flame **238**, 111917 (2022).
[34]M. Reith, A. Gruber, F. A. Williams, and J. H. Chen, "The effect of pressure on ammonia/hydrogen/nitrogen premixed flames in intense sheared turbulence, vol. 66, paper no: 17," in 74th Annual Meeting of the APS Division of Fluid Dynamics, 2021.